Springer

KSME

Journal of Mechanical Science and Technology 26 (10) (2012) 3009~3016
www.springerlink.com/content/1738-494x
DOI 10.1007/s12206-012-0817-5

Modeling and analysis of rotating plates by using self-sensing active constrained layer damping †

Zhengchao Xie*, Pak Kin Wong and Ian Ian Chong

Department of Electromechanical Engineering, University of Macau, Macau SAR, China

(Manuscript Received June 17, 2011; Revised December 15, 2011; Accepted May 2, 2012)

Abstract

This paper proposes a new finite element model for active constrained layer damped (CLD) rotating plate with self-sensing technique. Constrained layer damping can effectively reduce the vibration in rotating structures. Unfortunately, most existing research models the rotating structures as beams that are not the case many times. It is meaningful to model the rotating part as plates because of improvements on both the accuracy and the versatility. At the same time, existing research shows that the active constrained layer damping provides a more effective vibration control approach than the passive constrained layer damping. Thus, in this work, a single layer finite element is adopted to model a three-layer active constrained layer damped rotating plate. Unlike previous ones, this finite element model treats all three layers as having the both shear and extension strains, so all types of damping are taken into account. Also, the constraining layer is made of piezoelectric material to work as both the self-sensing sensor and actuator. Then, a proportional control strategy is implemented to effectively control the displacement of the tip end of the rotating plate. Additionally, a parametric study is conducted to explore the impact of some design parameters on structure's modal characteristics.

Keywords: Damping; Active control; Rotating plate; Finite element method (FEM)

1. Introduction

Constrained layer damping (CLD) is an effective approach for vibration controls. The fundamental mechanism of CLD is that the relative motion of two face layers leads to the deformation of the damping layer; the energy consumed through the deformation of the damping layer results in the damping effects. Currently, relatively large damping ratios can be achieved through a wide range of available viscoelastic materials.

In literature, extensive investigations have been conducted on constrained layer damping for beam structures. These researches widely employed an assumption proposed by Ross, Ungar and Kerwin (RUK) [1] that there is only shear deformation (pure shear) in the damping layer. In this assumption, the two face layers are treated as Euler-Beams while the core layer only experiences shear deformation. The motions associated with this assumption are illustrated in Fig. 1. For the convenience of the discussion, two face layers are called the constraining layer and the base layer respectively in this paper, while the middle layer is called the core layer. The layers are also denoted by numbers 1, 2 and 3, respectively, throughout this work. The displacements u_1 and u_3 are employed to represent the longitudinal displacements of face layer 1 and 2 respectively. w is utilized to denote the transverse displacement of sandwich structure, which is identical for each of the three layers. Shear deformation in the core layer is determined from the relative motion between u_1 and u_3.

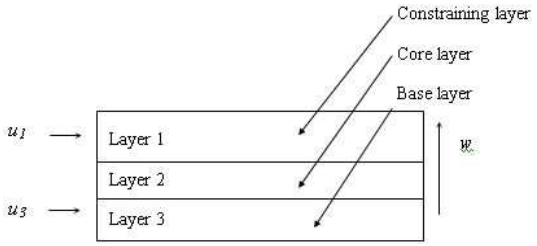

Fig. 1. RUK model displacements for a CLD sandwich beam chart.

While the assumptions described above are widely used, they are not always valid in certain structures when RKU model is employed. Rao [2] studied the problem using the same transverse displacement assumption as that in Ref. [1] but with additional assumptions that the longitudinal displacement varies linearly across the thickness of each layer, and the displacement is continuously across the layer connections. In that work, all of three layers are treated as Ti-

*Corresponding author. Tel.: +853 83978471, Fax.: +853 28838314
E-mail address: zxie@umac.mo
† Recommended by Associate Editor Vikas Tomar

moshenko beams instead of Euler beams used in the RKU model. Zapfe and Lesieutre [3] presented a beam finite element that can be regarded as the finite element implementation of the Rao's model. In addition to the passive constrained layer damping (PCLD), the active constrained layer damping (ACLD) approach has been shown that can bring more damping into the structure [4]. In ACLD technique, a voltage is applied on the piezoelectric constraining layer to generate active force. Gao and Liao [5] implemented self-sensing ACLD approach based on the work of Dosch and Inman [6]. In self-sensing ACLD approach, the piezoelectric constraining layer works as both the sensor and actuator, and a bridge circuit [6] is used to extract the sensed voltage from measured signal. One of advantages for this approach is that it can achieve the true collocated control which means the control systems is unconditionally stable [7].

Recently constrained layer damping is employed for the vibration suppressions of rotating structures, which has wide applications in industries such as wind turbines, helicopters, and vessels. Rotating beams, as simplification of rotating plates, have been extensively investigated, including fundamental dynamics [8]. Yoo and Pieere [9] studied the dynamics of rotating bare plates using analytical approach. Based on the work in [9], Liu and Hong [10] developed a plate finite element model for a rotating bare plate. Fung and Yau [11] studied ACLD application on rotating beam, and Shen [12] gives a work-energy relation of a self-sensing ACLD rotating beam. Liu et al. [13] extended their own work in Ref. [10] to active control of constrained layer damped rotating plates through finite element approach. It is worth noting that all of the work mentioned here utilized the same assumptions as those in RKU model that only shear strain exists in the core layer and extension strain in the constraining and base layers.

In this research, a plate finite element is employed to model the multi-layer rotating plates. This plate finite element model extends previous research from beam to plate, and it is expected that more possible types of damping can be captured for practical rotating plate analysis due to the proposed displacement field. This feature overcomes the over-simplification in previous works. Also, this plate finite element model can be extended to multi-layer (more than three) rotating plates conveniently. Then, a proportional control strategy is implemented with a self-sensing constraining layer, which means the piezoelectric constraining layer works as both the sensor and the actuator. The model is validated and a comprehensive parametric study is conducted to illustrate impacts of different design parameters on modal characteristics of ACLD rotating plates.

2. Finite element modeling

2.1 Assumptions and kinematics relations

Prior to introducing the rotating plate finite element model, the assumptions as those in Ref. [2] should be introduced. Note that the assumptions in Ref. [2] are for beams.

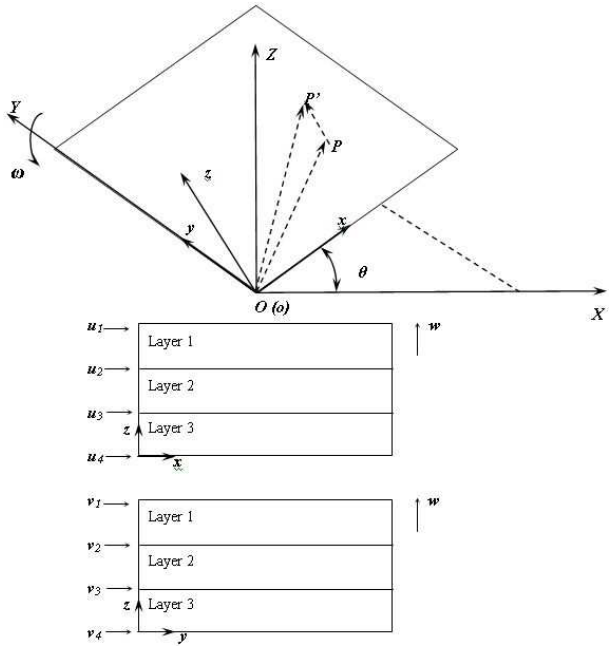

Fig. 2. Proposed displacement field.

(1) The transverse displacements of all three layers are equal.

(2) The longitudinal displacement is linearly distributed across the thickness of each layer.

(3) There is no slip between the layers.

The rotating plate is modeled in this work based on above assumptions. Fig. 2 shows the proposed displacement field for the rotating plate with angular velocity ω. w is the transverse displacement for all of the three layers. ui and vi are the longitudinal displacements at the contacting surfaces of different layers along the x and y axes, respectively. The longitudinal displacements of each layer vary linearly across the thickness of each layer. Note that there are two coordinate systems in Fig. 2, a rotating coordinate system o-xyz attached to the rotating plate, and a global coordinate system O-XYZ that is fixed without rotation. The transformation matrix between two coordinate systems is defined as in Ref. [10]:

$$A=\begin{bmatrix}\cos\theta & 0 & -\sin\theta\\ 0 & 1 & 0\\ \sin\theta & 0 & \cos\theta\end{bmatrix}. \tag{1}$$

Taking an arbitrary point on the rotating plate which moves from P to P' after the deformation, the

$$OP'_{xyz}=\begin{bmatrix}x\\ y\\ 0\end{bmatrix}+\begin{bmatrix}u\\ v\\ w\end{bmatrix}+\begin{bmatrix}-\int_0^x(\frac{\partial w}{\partial x})^2dx\\ -\int_0^y(\frac{\partial w}{\partial y})^2dy\\ 0\end{bmatrix}. \text{ The term } \begin{bmatrix}-\int_0^x(\frac{\partial w}{\partial x})^2dx\\ -\int_0^y(\frac{\partial w}{\partial y})^2dy\\ 0\end{bmatrix}$$

is the so-called 'stiffening effect' [10], which are the coupling terms between the transverse displacement and the longitudinal displacement due to the centrifugal force of the rotation. The transformation of the displacement from the ***o-xyz*** coordinate system to O-XYZ coordinate system can be made as follows:

$$OP'_{XYZ} = A\left(\begin{bmatrix} x \\ y \\ 0 \end{bmatrix} + \begin{bmatrix} u \\ v \\ w \end{bmatrix} + \begin{bmatrix} -\int_0^x (\frac{\partial w}{\partial x})^2 dx \\ -\int_0^y (\frac{\partial w}{\partial y})^2 dy \\ 0 \end{bmatrix}\right). \quad (2)$$

With the proposed displacement field, kinetic and strain energy can be obtained respectively, based on that, the equations of motion can be derived.

2.2 Strain and kinetic energy

Given displacement field, the elastic strain energy of the *ith* layer in the rotating plate can be represented as:

$$V_i = \frac{1}{6}\iiint_{V_i} \begin{Bmatrix} E_i\left(\left(\frac{\partial u_i}{\partial x}\right)^2 + \frac{\partial u_i}{\partial x}\frac{\partial u_{i+1}}{\partial x} + \left(\frac{\partial u_{i+1}}{\partial x}\right)^2\right) + 3G_i\left(\frac{\partial w_i}{\partial x} - \frac{u_i - u_{i+1}}{2H_i}\right)^2 + 3 * E_i I_i \frac{\partial^2 w}{\partial x^2} \\ + E_i\left(\left(\frac{\partial v_i}{\partial x}\right)^2 + \frac{\partial v_i}{\partial x}\frac{\partial v_{i+1}}{\partial x} + \left(\frac{\partial v_{i+1}}{\partial x}\right)^2\right) + 3G_i\left(\frac{\partial w_i}{\partial x} - \frac{v_i - v_{i+1}}{2H_i}\right)^2 \end{Bmatrix} dv, \quad (3)$$

where H_i is the thickness of *ith* layer.

The kinetic energy is dependent on structure's motion. Taking the time derivative of displacement OP'_{XYZ} in Eq. (3) gives:

$$OP'_{XYZ} = \dot{A}\begin{bmatrix} x + u - \int_0^x (\frac{\partial w}{\partial x})^2 dx \\ y + v - \int_0^y (\frac{\partial w}{\partial y})^2 dy \\ w \end{bmatrix} + A\begin{bmatrix} \dot{u} - \frac{\partial}{\partial t}(\int_0^x (\frac{\partial w}{\partial x})^2 dx) \\ \dot{v} - \frac{\partial}{\partial t}(\int_0^y (\frac{\partial w}{\partial y})^2 dy) \\ \dot{w} \end{bmatrix}. \quad (4)$$

The kinetic energy of the *ith* layer then can be calculated as:

$$T_i = \frac{1}{2}\rho_i \iiint_{V_i} ((\dot{u_i}^2 + \dot{v_i}^2 + \dot{w_i}^2) + \omega(2x\dot{w} + w\dot{u_i} + u_i\dot{w} - \dot{u_i}w - w\dot{u_i}) + \omega^2(x^2 + u_i^2 - x\int_0^x (\frac{\partial w}{\partial x})^2 dx + 2xu_i + w^2))dv \quad (5)$$

where $\omega = \dot{\theta}$ is the angular velocity of plate rotation.

2.3 Finite element discretization

As mentioned earlier, once the kinetic and the strain energy are obtained, the displacement field can be discretized using the new plate finite element. Fig. 3 shows the *ith* layer of the proposed new plate finite element. Here it is worth noting that the mid nodes are employed to avoid shear locking [3]. As a result, there are 25 degrees of freedom for the *ith* layer as shown in Fig. 3 and 41 degrees of freedom for all of three layers.

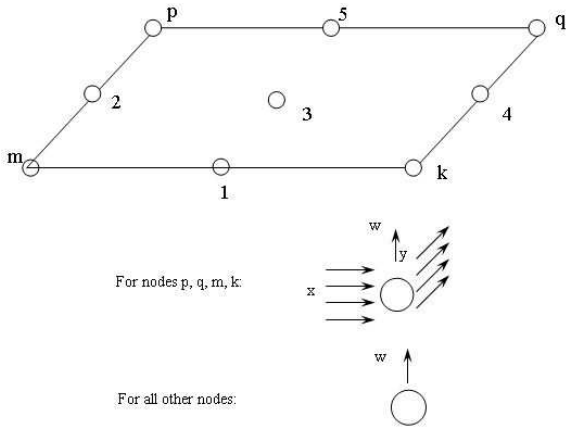

Fig. 3. Proposed new plate finite element.

The displacement vector of the *ith* layer with this new plate finite element becomes as follows:

$$\begin{aligned} q_i = [&u_{pi}\ u_{pi}\ v_{pi}\ v_{p(i+1)}\ w_p\ w_1\ u_{qi}\ u_{q(i+1)}\ v_{qi}\ v_{q(i+1)} \\ &w_q\ w_2\ w_3\ w_4\ u_{mi}\ u_{m(i+1)}\ v_{mi}\ v_{m(i+1)}\ w_m \\ &w_5\ u_{ki}\ u_{k(i+1)}\ v_{ki}\ v_{k(i+1)}\ w_k]^T. \end{aligned} \quad (6)$$

For the *ith* layer of plate finite element, the proposed displacement field (Fig. 3) can be organized as:

$$\begin{bmatrix} \mathrm{u} \\ \mathrm{v} \\ \mathrm{w} \end{bmatrix}_i = B\begin{bmatrix} u_i \\ u_{i+1} \\ v_i \\ v_{i+1} \\ w \end{bmatrix} = B\begin{bmatrix} F_1 \\ F_2 \\ F_3 \\ F_4 \\ F_5 \end{bmatrix} q_i = BFq_i = Nq_i \quad (7)$$

and the dimensions of matrix B and F are 3×5 and 5×25, respectively. Both matrixes are given as follows:

$$B = \begin{bmatrix} \frac{\mathrm{z}}{\mathrm{H_i}} & 1-\frac{\mathrm{z}}{\mathrm{H_i}} & 0 & 0 & 0 \\ 0 & 0 & \frac{\mathrm{z}}{\mathrm{H_i}} & 1-\frac{\mathrm{z}}{\mathrm{H_i}} & 0 \\ 0 & 0 & 0 & 0 & 1 \end{bmatrix} \quad (8)$$

where z and H_i respectively are the transverse coordinate and the thickness of the *ith* layer

$$F=\begin{bmatrix} n_1 & 0 & 0 & 0 & 0 & n_2 & 0 & 0 & 0 & 0 & 0 & 0 & n_3 & 0 & 0 & 0 & 0 & n_4 & 0 & 0 & 0 \\ 0 & n_1 & 0 & 0 & 0 & 0 & n_2 & 0 & 0 & 0 & 0 & 0 & 0 & n_3 & 0 & 0 & 0 & 0 & n_4 & 0 & 0 \\ 0 & 0 & n_1 & 0 & 0 & 0 & 0 & n_2 & 0 & 0 & 0 & 0 & 0 & 0 & n_3 & 0 & 0 & 0 & 0 & n_4 & 0 \\ 0 & 0 & 0 & n_1 & 0 & 0 & 0 & 0 & n_2 & 0 & 0 & 0 & 0 & 0 & 0 & n_3 & 0 & 0 & 0 & 0 & n_4 \\ 0 & 0 & 0 & 0 & b_1 & b_2 & 0 & 0 & 0 & b_3 & b_4 & b_5 & b_6 & 0 & 0 & 0 & b_7 & b_8 & 0 & 0 & b_9 \end{bmatrix}, \tag{9}$$

where $n_1 - n_4$ are the shape functions for the longitudinal displacement and $b_1 - b_9$ are the shape functions for the transverse displacement. Because they can be calculated according to many finite element textbooks, they are not given in detail in this work.

Also, the displacement vector q_i can be assembled to the total displacement vector q of the whole plate finite element with three layers:

$$q = \sum_{i=1}^{3} TR_i q_i \tag{10}$$

where TR_i is the map matrix of the *ith* layer. TR_i is a $n \times 25$ matrix and n is the total number of degrees of freedom in the plate finite element (41 for three layers). While CLD rotating plate structure with three layers is employed as a physical base for derivation of motion equations in this paper, it can be easily extended to CLD structure with multiple layers using this modeling approach.

Substituting Eq. (7) into Eqs. (2), (3) and (5), and neglecting high order terms, the kinetic and strain energy of the *ith* layer can be reorganized as:

$$\begin{aligned} V_i = \frac{1}{6}\iiint_{V_i} & (E_i q_i^T \left((\frac{\partial F_1}{\partial x})^T (\frac{\partial F_1}{\partial x}) + (\frac{\partial F_1}{\partial x})^T (\frac{\partial F_1}{\partial x}) + (\frac{\partial F_2}{\partial x})^T (\frac{\partial F_2}{\partial x}) \right) q_i \\ & + E_i q_i^T \left((\frac{\partial F_3}{\partial y})^T (\frac{\partial F_3}{\partial y}) + (\frac{\partial F_3}{\partial y})^T (\frac{\partial F_4}{\partial y}) + (\frac{\partial F_4}{\partial y})^T (\frac{\partial F_4}{\partial y}) \right) q_i \\ & + 3G_i q_i^T \left(\frac{\partial F_5}{\partial x} - \frac{F_1 - F_2}{2H_i} \right)^T \left(\frac{\partial F_5}{\partial x} - \frac{F_1 - F_2}{2H_i} \right) q_i \\ & + 3G_i q_i^T \left(\frac{\partial F_5}{\partial y} - \frac{F_3 - F_4}{2H_i} \right)^T \left(\frac{\partial F_5}{\partial y} - \frac{F_1 - F_2}{2H_i} \right) q_i) dv \end{aligned} \tag{11}$$

$$\begin{aligned} T_i = \frac{1}{2}\rho_i \iiint_{V_i} & (\dot{q}_i^T N^T N \dot{q}_i + \omega(2xN_3 q_i + \dot{q}_i^T N_3^T N_1 q_i + q_i^T N_1^T N_3 \dot{q}_i^T \\ & - \dot{q}_i^T N_1^T N_3 q_i - \dot{q}_i^T N_3^T N_1 q_i) + \omega^2 (x^2 + q_i^T N_1^T N_1 q_i \\ & + q_i^T N_1^T N_1 q_i - x q_i^T \int_0^x (\frac{\partial N_3}{\partial x})^T (\frac{\partial N_3}{\partial x}) dx q_i + 2x N_1 q_i) dv . \end{aligned} \tag{12}$$

2.4 Self-sensing ACLD

The piezoelectric constraining layer acts as both the sensor and the actuator. The sensed voltage is feedback through a proportional gain to apply a voltage over the constraining layer to generate active force. There are two assumptions on the ACLD in this work. First the viscoelastic layer is fully covered by the piezoelectric constraining layer, and second the applied voltage is homogenous over the whole surface of the constraining layer.

The constitutive equation of piezoelectric material is given in the book of Moheimani et al. [14] and shown as follows:

$$\sigma = C^{-1}\varepsilon + dE \tag{13}$$

and

$$D = d^T \varepsilon + eE \tag{14}$$

where σ, ε, d, E, C, e, and D are the stress, strain, matrix of piezoelectric constants, applied electric field, matrix of elastic compliance, permittivity matrix, and electric displacement on the surface of the constraining layer, respectively. Then, the accumulated charges due to the deformation can be calculated as:

$$D = \iint_A d^T C \varepsilon_{\bar{z}} dxdy \tag{15}$$

where $\bar{z}$ is the transverse coordinate at the mid-plane of the constraining layer as given in the work of Hwang et al. [15], and the sensed voltage can be calculated accordingly as:

$$V_s = \frac{D}{C_p} \tag{16}$$

where C_p is the capacitance of the constraining layer.

Because the proportional control is used in this work, the applied control voltage V_a can be easily calculated as $V_a = K_p V_s$, and K_p is the proportional gain. Then, generated active force can be calculated by

$$F_c = \iiint_{v_1} \frac{\varepsilon^T C dV_a}{H_1} dxdydz . \tag{17}$$

Note that the terms for active force should be discretized to be integrated into the finite element model.

2.5 Equations of motion

With Eqs. (11), (12) and (17), the global equations of motion for the rotating plate can be obtained using Lagrange formula as follows;

$$[M]\ddot{q} + [C]\dot{q} + ([K] + [K]_p)q = f \tag{18}$$

where

$$\begin{aligned} M &= \iiint_V N^T N dv \\ C &= 2\omega \iiint_V (N_3^T N_1 - N_1^T N_3) dv \\ K &= K_1 - \omega^2 \iiint_V (N_1^T N_3 + N_3^T N_1) dv + \omega^2 RP \\ &\quad + \dot{\omega} \iiint_V (N_3^T N_1 - N_1^T N_3) dv \\ f &= \omega \iiint_V x N_1 dv - \dot{\omega} \iiint_V x N_3 dv . \end{aligned} \tag{19}$$

Table 1. Comparison between results of new plate finite element model and Ref. [11] with 30 rpm rotation speed.

Modes	Frequency (Hz)		Difference (%)	Damping ratio (%)		Difference (%)
	New FE model	Ref. [11]		New FE model	Ref. [11]	
First bending	20.2	20.2	0	3.8	3.8	0
Second bending	106.1	104.0	2.0	2.3	2.3	0
First torsion	186.3	N/A	N/A	0.49	N/A	N/A
Third bending	290.1	277.0	4.5	1.15	1.23	7.0

The integration domain V is the volume of three-layer plate. $[K]_p$, the stiffness matrix, comes from the proportional control, and K_1 and RP are the elastic strain stiffness in *o-xyz* coordinate system and stiffening matrix, respectively. As the same coupling terms between the transverse and longitudinal displacements are used, the derivation of RP in this work is similar to that in Ref. [13]. It is worth noting that the proposed displacement field and derivation approach in present study are different from those in Ref. [13], where the bare rotating plate is investigated in the latter while three layer CLD structure is considered in this study. Here, the Lagrange formula is applied to each layer (q_i) first, and then the local equation of motion of each layer is assembled to form the global Eq. (18). It can be seen that this approach can be easily extended to CLD structure with multiple layers (more than three layers), and this newly proposed model could be adopted in practical design of rotating machines, such as wind turbine blades.

3. Validation of the finite element model

In this section, the developed finite element model is validated using data from open literature, upon which, further parametric study can be performed. In this regard, we consider an identical 0.3 m long rotating and constrained layer damped sandwich beam as studied in Ref. [11]. The first three bending modes of this beam are calculated using the newly proposed finite element model and compared with those in Ref. [11], where the rotation speed is set at 30 revolutions per-minute (rpm). One can see from Table 1 that all of the first three modes obtained from the new finite element model match pretty well with those in Ref. [11]. It is interesting to note from Table 1 that the developed new finite element model is able to identify the first torsion mode while the beam model in Ref. [11] is not, and this is an advantage of plate model over the beam model. With the validated active constrained layer damped plate model, it is possible to conduct the parametric study to check their impact on the model modal characteristics.

4. Parametric studies

In this section several parameters includes the proportional control gain K_p, the thickness of constraining layer H_1, the thickness of damping layer H_2, the width of the plate L_2, and the rotation speed *rpm* are selected. Then, the impacts of these parameters on the frequency response function (FRF) are studied because it is necessary to check the damped response [16], and the first three natural frequencies and damping ratios are studied as well. The parameters used in this study are based on a baseline configuration listed in Table 2, and their variations of configurations (configurations from 1 to 5) are listed as in Table 3. When each selected parameter varies in the study, all other parameters are kept as the same as those in the baseline configuration.

In order to check the impacts of different values of K_p on the frequency response function, an impulse in time domain is applied at a corner point as shown in Fig. 4. In this way, both the bending and torsional modes can be captured. Apparently, the response at this point is the FRF of this point. Figs. 5-7 show the FRF over the first three modes function, and it can be seen that when K_p increases, the amplitudes of FRF at the

Table 2. Parameters for the baseline configuration in parameter study.

Parameters	Value	Parameters	Value
Thickness 1	0.000762 m	Shear modulus 1	24.96 Gpa
Thickness 2	0.00025 m	Shear modulus 2	0.2615 Mpa
Thickness 3	0.002286 m	Shear modulus 3	27.3 Gpa
Young's modulus 1	64.9 Gpa	Density 1	7600 kg/m^3
Young's modulus 2	29.8 Mpa	Density 2	1250 kg/m^3
Young's modulus 3	71 Gpa	Density 3	2700 kg/m^3
Width	0.15 m	Length	0.3 m
Rotation speed	240 rpm	loss factor	0.38
Kp	10		

1: Constraining layer
2: Damping layer
3: Base material

Table 3. Different configurations in parameter study.

Parameters	Config. 1	Config. 2	Config. 3	Config. 4	Config. 5
Thickness 1	0.0001 m	0.00025 m	0.00045 m	0.00065 m	0.000762 m
Thickness 2	0.00025 m	0.0005 m	0.00075 m	0.001 m	0.0012 m
Width	0.15 m	0.3 m	0.4 m	0.5 m	0.6 m
Kp	2	10	50	100	200
Rotation speed	60 rpm	120 rpm	180 rpm	240 rpm	300 rpm

1: Constraining layer
2: Damping layer
3: Base material

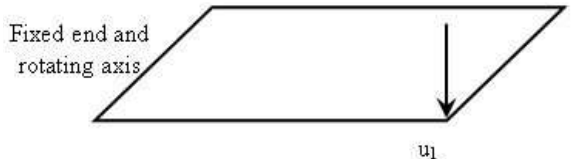

Fig. 4. Impulse applied on the corner point of the rotating plate.

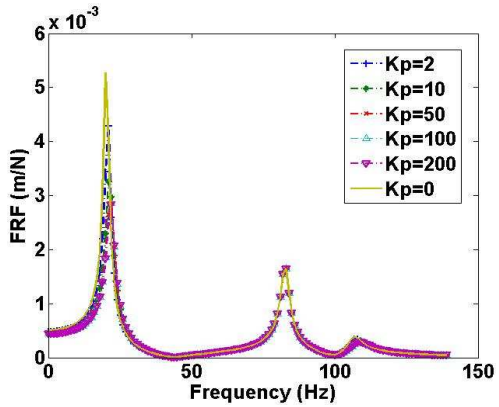

Fig. 5. FRF over the first three modes.

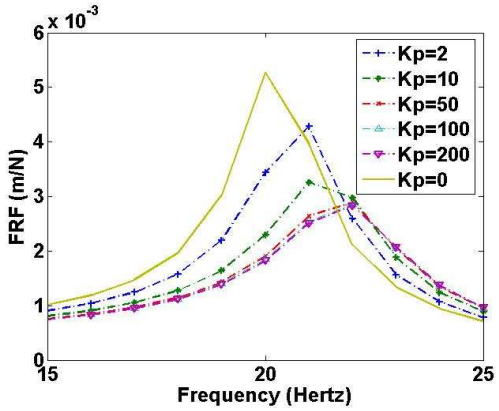

Fig. 6. FRF at the first mode.

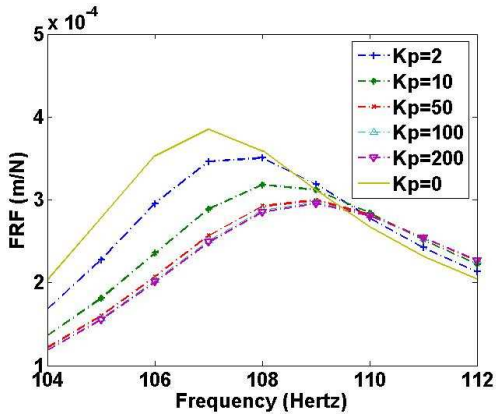

Fig. 7. FRF at the third mode.

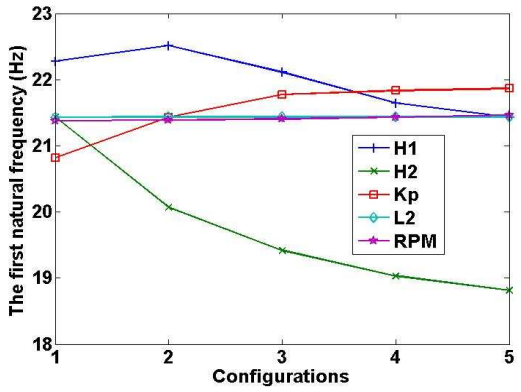

Fig. 8. Variations of the first natural frequency with regard to different parameters.

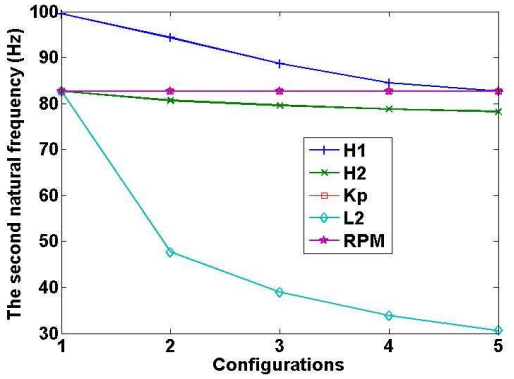

Fig. 9. Variations of the second natural frequency with regard to different parameters.

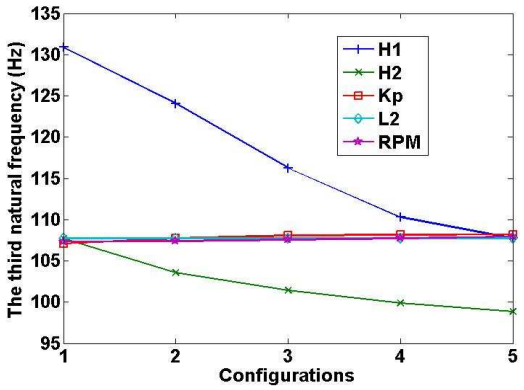

Fig. 10. Variations of the third natural frequency with regard to different parameters.

first and the third modes drop and these two resonant frequencies shift to right (increase). This is due to the increase of stiffness and damping ratio with higher K_p value. However, for the second mode which is a torsional mode, the K_p has no much impact on it, and this is due to the assumptions of uniform voltage over the surface of constraining layer, and fully coverage of damping and constraining layer. This means the proposed proportional control strategy in this work can effective suppress the bending vibration, but not so much for torsional vibration [17]. Some additional numerical solution for similar work can be found in Refs. [18-23].

Figs. 8-10 show the variations of first three nature frequencies in different configurations. It can be seen that the first nature frequency goes up as the K_p increases, and goes down as the thickness of constraining layer and damping layer increase. This can be explained as the increase of stiffness and mass of the plate, respectively. However, same as discussed before, the K_p value doesn't have much impact on the sec-

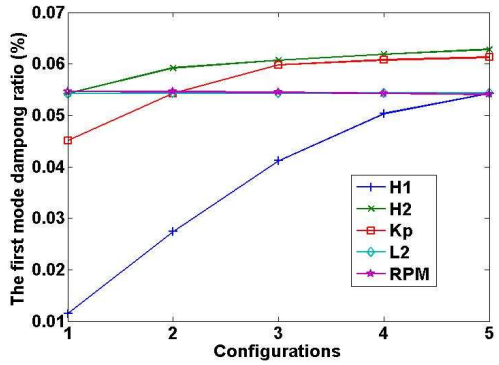

Fig. 11. Variations of the first mode damping ratio with regard to different parameters.

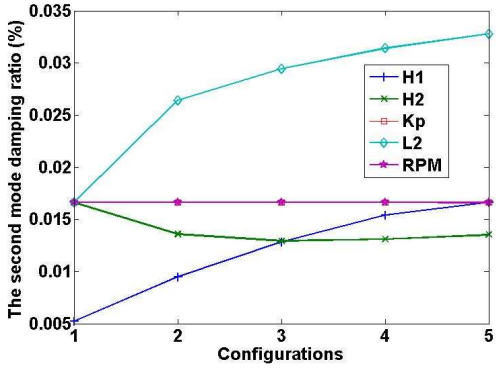

Fig. 12. Variations of the second mode damping ratio with regard to different parameters.

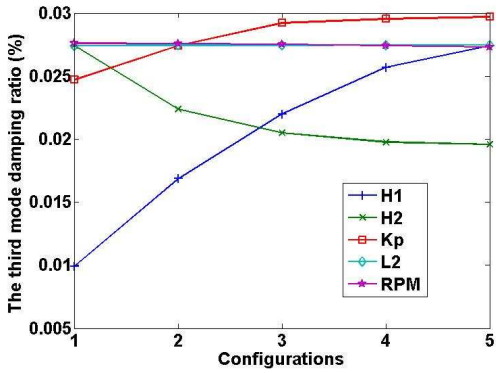

Fig. 13. Variations of the third mode damping ratio with regard to different parameters.

ond mode. Due to the 'stiffening effect', the first three nature frequencies increase with higher rotation speeds. Note that this sharp increase hardly can be seen in Figs. 8 to 10 due to the plot scale setting. Also, it can be seen that increasing the width of the plate leads to a lower natural frequency at the second mode, which is a torsional mode, and this means the torsional stiffness of the plate drops.

Figs. 11-13 illustrated the impacts of selected parameters on the first three mode damping ratios. When K_p increases, the damping ratios of the first and third mode increase accordingly, while the second mode damping ratio keeps almost unchanged which agrees with the FRF shown previously. Higher constraining layer thickness can increase damping ratios at all three modes, and wider the plate can only leads to a higher damping ratio at the second mode and has no obvious impact on the other two modes. Also, damping ratios at all three modes drop with higher rotation speeds. It seems that the damping ratios at the first three modes have same trends to either increase or decrease when most selected parameters change, however, it is interesting to note that it is not so for the damping layer thickness. It can be seen that as the damping layer thickness increases, the first mode damping ratio increases while the other two modes damping ratios decrease.

5. Conclusions

A new self-sensing active constrained layer damped plate finite element model is developed for rotating plates. The proposed displacement field and degrees of freedom enable this finite element model to capture the shear and extension deformation in all three layers. This model is validated using the results of natural frequencies and damping ratios from published literature, and then the validated model is employed for parametric study. Results show that the active constrained layer damping works more effectively than the passive constrained layer damping. From the parameter study, it can be seen that higher proportional gains can apparently lead to higher damping ratios and slightly increase the natural bending frequencies, while has no much impact on the torsion mode. Also, higher core and constraining layer thickness cause lower natural frequencies. Not surprisingly that wider plate leads to lower frequency and higher damping ratio of the torsional mode. When rotation speed goes up, the natural frequencies go up as well because the stiffening effect is strengthened, while the damping ratios drop down. The finite element model developed in this study provides a generic method for dynamic characteristic investigation of rotating plates with active constrained layer damping. In the future, this model can be used to conduct design optimizations of active constrain layer damped rotating plates, and also can be treated as a starting point for the fluid-structure coupling analysis on rotating structures with complex geometries such as wind turbines.

Acknowledgment

This work is supported by the start-up research fund from the University of Macau Research Committee under the RC Ref. Number: SRF016/09-10S/ZCX/FST.

References

[1] D. Ross, E. E. Ungar and E. M. Kerwin, Damping of plate flexural vibrations by means of viscoelastic laminae, *ASME Annual Meeting Structural Damping*, New York, USA (1959) 49-88.

[2] D. K. Rao, Vibration of short sandwich beams, *Journal of Sound and Vibration*, 52 (2) (1977) 253-263.

[3] J. A. Zapfe and G. A. Lesieutre, A discrete layer finite element for the dynamic analysis of composite sandwich beams with integral damping layers, *Computer and Structures*, 70 (6) (1997) 647-666.
[4] A. Baz and J. Ro, Vibration control of plates with active constrained layer damping, *Smart Material and Structures*, 5 (3) (1996) 272-280.
[5] J. X. Gao and W. H. Liao, Vibration analysis of simply supported beams with enhanced self-sensing active constrained layer damping treatments, *Journal of Sound and Vibration*, 280 (1-2) (2005) 329-357.
[6] J. Dosch and D. Inman, A self-sensing piezoelectric actuator for collocated control, *Journal of Intelligent Material Systems and Structures,* 3 (1) (1992) 166-185.
[7] A. Baz and J. Ro, Vibration control of plates using self-sensing active constrained layer damping, *Journal of Vibration and Control*, 8 (6) (2002) 833-845.
[8] Y. A. Kulief, Vibration frequencies of a rotating tapered beam with end mass, *Journal of Sound and Vibration*, 134 (1) (1989) 87-97.
[9] H. H. Yoo and C. Pieere, Modal characteristic of a rotating rectangular cantilever plate, *Journal of Sound and Vibration*, 259 (1) (2003) 81-96.
[10] J. Liu and J. Hong, Geometric nonlinear formulation and discretization method for a rectangular plate undergoing large overall motions, *Mechanics Research Communications,* 32 (5) (2005) 561-571.
[11] E. H. K. Fung and D. T. W. Yau, Vibration of a rotating flexible arm with ACLD treatment, *Journal of Sound and Vibration*, 269 (1-2) (2004) 165-182.
[12] I. Y. Shen, A variational formulation, a work-energy relation and damping mechanism of active constrained layer treatments, *Journal of Vibration and Acoustics*, 119 (2) (1997) 192-199.
[13] L. Liu, Z. Zhang and H. Hua, Dynamic characteristics of rotating cantilever plates with active constrained layer damping treatments, *Smart Materials and Structures*, 16 (5) (2007) 1849-1856.
[14] S. O. R. Moheimani and A. J. Fleming, *Piezoelectric Transducers for Vibration Control and Damping*, Springer Press, New York, USA (2006).
[15] W. S. Hwang, H. C. Park and W. Hwang, Vibration control of a laminated plate with piezoelectric sensor/actuator: finite element formulation and modal analysis, *Journal of Intelligent Material Systems and Structures*, 4 (3) (1993) 317-329.
[16] D. Laxalde, F. Thouverez and J. P. Lombard, Forced response analysis of integrally bladed disks with friction ring dampers, *Journal of Vibration and Acoustics- ASME Transactions*, 132 (1) (2010) 011013.1-011013.9.
[17] A. Baz and J. Ro, Vibration control of plates using self-sensing active constrained layer damping networks, *Journal of Vibration and Control*, 8 (6) (2002) 833-845.
[18] S. Nadeem, N. S. Akbar and M. Y. Malik, Numerical solutions of peristaltic flow of a newtonian fluid under the effects of magnetic field and heat transfer in a porous concentric tube, *Zeitschrift fur Naturforschung*, 65a (2010) 1-12.
[19] S. Nadeem and N. S. Akbar, Numerical solutions of peristaltic flow of a jeffrey-six constant fluid with variable MHD, *Zeitschrift fur Naturforschung*, 65a (2010) 19.
[20] S. Nadeem, N. S. Akbar and M. Y. Malik, Exact and numerical solutions of a micro polar fluid in a vertical annulus, *Numerical Methods for Partial Differential Equation*, 26 (6) (2010) 1660-1674.
[21] S. Nadeem and N. S. Akbar, Exact and numerical simulation of peristaltic flow of a non-newtonian fluid with inclined magnetic field in an endoscope, *International Journal for Numerical Methods in Fluids*, 66 (7) (2011) 919-934.
[22] S. Nadeem and N. S. Akbar, Numerical Solutions of peristaltic flow of williamson fluid with radially varying mhd in an endoscope. *International Journal for Numerical Methods in Fluids*, 66 (2) (2011) 212-220.
[23] S. Nadeem and N. S. Akbar, Numerical analysis of peristaltic transport of a tangent hyperbolic fluid in an endoscope, *Journal of Aerospace engineering*, 24 (3) (2011) 309-318.

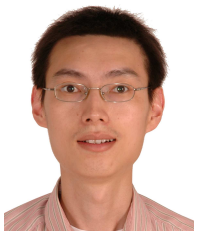

Zhengchao Xie received his B.Sc degree from Jilin University and M.Sc degree from Huazhong University of Science and Technology, both degrees are on automotive engineering. Dr. Xie got his Ph.D degree from University of Alabama and his research interests include vibration control, finite element method, and design optimization.

Pak Kin Wong is currently a Department Head of Electromechanical Engineering, University of Macau, Macao. He received his Ph.D degree in Mechanical Engineering from The Hong Kong Polytechnic University in 1997. His research interests include automotive engineering, fluid transmission & control, engineering applications of artificial intelligence and mechanical vibration.

Ian Ian Chong received his B.Sc degree from Shanghai Jiaotong University, and M.Sc degree from University of Macau. His research interests include mechanical vibration, application of constrained layer damping and design optimization.